International Journal of Applied Earth Observation and Geoinformation 139 (2025) 104548

Contents lists available at ScienceDirect

International Journal of Applied Earth Observation and Geoinformation

journal homepage: www.elsevier.com/locate/jag

Accounting for temporal and spatial autocorrelation to examine the effects of climate change on vegetation greenness trend in China

Lingwei Chen [a], Likai Zhu [a,*], Cuiyutong Yang [a], Zizhen Dong [a], Rui Huang [a], Jijun Meng [b], Min Liu [a]

[a] *Key Laboratory of Geographic Information Science, Ministry of Education, School of Geographic Sciences, East China Normal University, Shanghai 200241, China*
[b] *Key Laboratory of Earth Surface Processes of Ministry of Education, College of Urban and Environmental Sciences, Peking University, China*

ARTICLE INFO

Keywords:
Vegetation greenness trend
Climate change
Autocorrelation
Statistical test
China

ABSTRACT

Trend and attribution analysis of vegetation greenness is crucial to explain and predict ecosystem responses to climate change. The common practice to detect and explain greenness pattern from remote sensing time series is mostly based on pixel-by-pixel analysis, which often fails to account for spatial autocorrelation and may lead to spurious patterns. Here we applied the Partitioned Autoregressive Time Series (PARTS) method to the Normalized Difference Vegetation Index-3rd generation (NDVI3g) data and multiple climate datasets, and examined the climate effects on greenness trend in China. This method considers temporal and spatial autocorrelation structure, and aggregates pixel information to rigorously test the hypotheses about regional patterns. The results showed that greenness trends were strongly impacted by climate change, environmental background and their interactions. In regions with lower greenness, higher temperature, more precipitation and soil moisture, and lower vapor pressure deficit (VPD), the greening rate tends to be higher. For the whole China, long-term trends of temperature ($P < 0.05$) and soil moisture ($P < 0.05$) made significantly negative effects on greenness trend, while trend of precipitation ($P < 0.05$) and VPD ($P < 0.001$) made significantly positive impacts. But their effects strongly interacted with environmental background. The overall positive VPD impact was significantly enhanced with an increase in VPD level ($P < 0.001$), which was also supported by the significantly positive VPD impact in the northwestern arid regions (high VPD) and the significantly negative impact in the tropical and subtropical areas (low VPD). In the cold ecosystems, the change in soil moisture made significantly negative effect on greenness trend. This study provides new insights into the driving mechanisms of greenness change, which is useful to inform ecosystem modeling to make accurate predictions. Moreover, the analysis framework with PARTS method could be effectively applied to other regions or to analyzing other ecosystem responses to climate change.

1. Introduction

Terrestrial vegetation plays vital roles in the coupled human-environment system (DeFries, 2008). Vegetation absorbs CO_2 through photosynthesis, influencing the carbon sequestration capacity and the global carbon budget (Friedlingstein et al., 2023). It impacts hydrological cycles through the water transfer between the land and the atmosphere due to evapotranspiration and leaf interception (Gentine et al., 2019). Vegetation could provide animals with habitats and food resources to maintain biodiversity (Radeloff et al., 2019), and supply various ecosystem services that are closely linked to human well-being such as crop and wood production (Bennett et al., 2009). Due to climate change and land use activities, terrestrial vegetation is undergoing pronounced changes, causing great consequences on human-environment systems (Piao et al., 2020). For example, the greening trend of global vegetation leads to an increase in terrestrial carbon sinks, which has offset approximately 29 % of anthropogenic CO_2 emissions (Friedlingstein et al., 2023; Zhu et al., 2016). Therefore, detection and attribution of greenness change pattern is crucial for understanding the energy, water, and biogeochemical cycles across terrestrial landscapes, and assessing the delivery of ecosystem services that linked with human wellbeing (Miralles et al., 2025).

Due to the unique optical spectrum of vegetation, the long-term remote sensing time series are widely used to analyze vegetation

* Corresponding author at: Hekou Building A845, No. 500 Dongchuan Road, Minhang District, Shanghai200241, China.
E-mail address: lkzhu@geo.ecnu.edu.cn (L. Zhu).

https://doi.org/10.1016/j.jag.2025.104548
Received 7 November 2024; Received in revised form 20 March 2025; Accepted 16 April 2025

greenness trends at different spatial and temporal scales (Piao et al., 2020). The common practice of doing so consists of two steps: (i) conducting trend analysis by pixel, and making maps of trends at predefined significance levels from which we visually describe where the significant changes occur (de Beurs and Henebry, 2007); (ii) averaging the trends of pixels to reflect the overall trend for a geographical unit (e.g., a region, climate zone, or ecosystem type)(Zhu et al., 2020). As regarding the first step, the commonly used trend detection methods include Mann-Kendall test (MK) with Sen's slope, Least Squares (LS) method, and Size-Robust Trend analysis (SR) (Fensholt et al., 2012; Xu et al., 2013). However, MK and LS methods do not consider the temporal autocorrelation in the time series, which may lead to increased type I error rate; SR considers temporal autocorrelation, but cannot insufficiently rejects null hypothesis (Ives et al., 2021). As regarding the second step, the overall greenness trend of a region from averaging pixel-level trends information is uncertain due to the spatial autocorrelation among pixels (Ives et al., 2021; Wadoux and Heuvelink, 2023). Therefore, a method that could account for spatial and temporal autocorrelation and enables to aggregate pixel information to test hypothesis of regional trend pattern is needed (Ives et al., 2021).

Attribution analysis is prerequisite for predicting greenness trend under future environmental change (Piao et al., 2020). To quantify the impacts of various natural and anthropogenic factors on greenness change, statistical methods are widely used including correlation analysis, regression analysis and more advanced methods such as random forests and Geodetector method (Shi et al., 2020; Zhao et al., 2018; Zhu et al., 2020). These methods can address specific challenges in attribution analysis of greenness change such as factor interactions (Zhu et al., 2020), and provide useful information about driving mechanisms (Piao et al., 2020). But many concerns remain in the analysis and have been neglected (Ives et al., 2021). First, correlation or regression analysis conducted at pixel level cannot infer the causes of greenness change at the regional level due to the same challenge as pixel-level trend analysis mentioned above (Wadoux and Heuvelink, 2023). Second, the current statistical methods often do not distinguish the effect of year-to-year fluctuations of driving factors and the effect of their long-term trends (Ives, 1995; Linscheid et al., 2020). Since the ecological processes that govern the year-to-year fluctuations in greenness may be fundamentally different from the processes that govern the long-term greenness trend, the short-term relationships which regression or correlation analysis focuses on could not be used to predict and explain the long-term greenness trend (Linscheid et al., 2020; Walker et al., 2020; Wolkovich et al., 2012). Terrestrial ecosystem modelling method accounts for complex ecological processes, and have advantages in quantifying the contributions of driving factors, and making future predictions (Pei et al., 2022; Zhang et al., 2022). For example, ecosystem models have shown that carbon dioxide concentration, climate change, land use change, and nitrogen deposition are the main driving factors of global vegetation greenness changes (Zhu et al., 2016). However, more often than not, statistical methods still play an important role in detecting the trends and examining the relationships from model simulation outputs (Zhang et al., 2022). Therefore, an attribution method that can examine the long-term relationships between the trends of greenness and climate factors and enables to aggregate pixel impact information to test regional patterns is needed (Ives et al., 2021; Linscheid et al., 2020).

The aforementioned issues and challenges in trend and attribution analysis from remote sensing data has been recognized and accounted for in several studies (Cortés et al., 2021; Xu et al., 2013; Zhou et al., 2001). Zhou et al. (2001) recognized early the role of spatial autocorrelation in analyzing change patterns from remote sensing, and developed metrics to measure spatial autocorrelation to assist in explaining change patterns. Cortés et al. (2021) pointed out that the commonly used pixel-based trend analysis might lead to higher rate of false positives and further cause the interpretation of spurious spatial patterns. A novel statistical method was then developed to correct the pixel trend by considering its neighboring pixels, and reduced the detected greening from 35.2 % to 15.3 % of the terrestrial land surface (Cortés et al., 2021). Although they give pixel-scale P-values corrected for spatial autocorrelation, they do not lead to map-scale statistical tests that aggregate the power from all pixels on a map (Ives et al., 2021; Ives et al., 2022). One more difficulty is the large data size of remote sensing time series, which limits the use of traditional spatial regression models or other advanced methods such as Geodetector (Ives et al., 2022; Zhu et al., 2020). For example, processing the matrix for storing spatial autocorrelation between each pair of millions of pixels is almost impossible (Ives et al., 2021). Given the above gaps, we employed the PARTS method to reanalyze the spatial patterns of greenness trend in China and their relationships with climate change. PARTS method can account for temporal and spatial autocorrelation in large remote sensing data and make a statistical test for regional pattern by aggregating pixel information from millions of pixels; it can also quantify the relationship between long-term trends of greenness and climatic factors (Ives et al., 2021; Ives et al., 2022). Moreover, understanding the greenness change in China is important because its largest greening rate has made substantial contributions to global carbon reduction efforts (Chen et al., 2019).We addressed the following research questions: (1) What is the overall greenness trend in China from 1982 to 2015? Is it significant? (2) Do the greenness trends differ significantly among different vegetation types and eco-geographical zones? What is the trend in each type/zone? (3) Do the greenness trends change significantly with in the gradients of environmental background? (4) How do the long-term trends in climatic factors influence greenness trends? (5) Do the impacts of climate change on greenness trends differ significantly among different eco-geographical zones and vegetation types? Section 3.1 provides the answers to research questions (1) and (2). Questions (3) and (4) are specifically examined in Section 3.2. The results related to research question (5) are shown in Section 3.3.

2. Data and methods

2.1. Data and preprocessing

2.1.1. NDVI dataset

Vegetation leaf has lower reflectance in the red satellite band due to photosynthetic activities, and higher reflectance in the near-infrared band due to spongy mesophyll (Zeng et al., 2022). Based on this rationale, NDVI is developed using spectrometric data at red and near-infrared bands as shown in Eq. (1):

$$\mathrm{NDVI} = \frac{\rho_{NIR} - \rho_{Red}}{\rho_{NIR} + \rho_{Red}} \tag{1}$$

where ρ_{Red} and ρ_{NIR} is the reflectance of red and near-infrared bands, respectively. NDVI curve could well capture the intra- and inter-annual variations of vegetation growth, photosynthetic activity, and greenness level so that NDVI has been widely used to analyze broad-scale vegetation dynamics (Piao et al., 2020).

Annual mean NDVI, calculated from the NDVI3g dataset, was used to analyze greenness trends (Pettorelli et al., 2005). The dataset is derived from the Advanced Very High Resolution Radiometer (AVHRR) image records that are formed from two AVHRR instruments, the AVHRR/2 that flew from July 1981 to November 2000 and the AVHRR/3 instrument that has flown since November 2000 (Pinzon and Tucker, 2014). These instruments are on board a series of NOAA satellites (NOAA 7, 9, 11, 14, 16, 17, and 18) (Li et al., 2023). An inter-calibration processing chain based on Bayesian methods were developed to minimize AVHRR/2 and AVHRR/3 NDVI incompatibilities and achieve good data consistency with the effects of calibration loss, orbital drift, volcanic eruptions, and other factors removed (Pinzon and Tucker, 2014). Compared to NDVI data products from other satellites such as MODIS, this one has longer time range from 1981 to 2015 at a spatial resolution of 0.0833° and a temporal resolution of approximately 15 days. The iterative

Savitzky-Golay (SG) filtering was applied to the NDVI time series to eliminate outliers and correct the lower NDVI values due to cloud contamination (Chen et al., 2004). First, the SG filter was applied to the raw NDVI time series to fit a new long-term change trend curve. Second, the new change trend curve was compared to the raw time series to determine the weight of each point. These weights would be used to calculate the fitting-effect index which determines when the iteration exits to get the best description of NDVI variations. Third, the outliers within raw time series indicated by lower weights were replaced with the values of fitted change trend curve, generating a new time series. Fourth, a new iteration was made based on the derived time series following the steps 1–3, and iteration would exit when the fitting-effect index achieved the minimum. Through this model, the processed NDVI curve approaches the upper envelope of original NDVI data, and gives the best description of plant growth curve. The detailed description of this method could be found in the paper by Chen et al (2004). Based on the improved NDVI time series, annual mean NDVI was calculated as the average of all NDVI observations within a calendar year (Pettorelli et al., 2005).

2.1.2. Climate datasets

Annual mean temperature, annual precipitation, annual mean VPD, annual mean soil moisture, and annual mean solar radiation were selected as potential climatic driving factors of vegetation greenness. Numerous studies have shown that these factors significantly impact vegetation dynamics in specific ecosystems(Hao et al., 2024; Nemani et al., 2003; Piao et al., 2020; Wu et al., 2015; Yuan et al., 2019).

Annual mean temperature and annual precipitation was calculated from the monthly temperature and precipitation data of China (Peng et al., 2019). The dataset was spatially downscaled from the 0.5-degree Climatic Research Unit (CRU) time series dataset with the climatology dataset of WorldClim using delta spatial downscaling. The WorldClim data show well capture climatology at high resolution, while the coarse-resolution CRU data have low bias in representing long-term variability. The rationale is to fuse the monthly anomaly time series of CRU temperature or precipitation with WorldClim climatology to generate long-term (1901–2023) and high-resolution (~1km) climate time series with high accuracy. Annual mean temperature was determined as the average of monthly temperature within a calendar year, and annual precipitation was defined as the sum of monthly precipitation.

Annual mean soil moisture was calculated from the monthly soil moisture data generated by the Global Land Data Assimilation System Version 2.0 (GLDAS-2.0) Noah land surface model L4 (Rodell et al., 2004). The GLDAS ingests satellite- and ground-based observational data products, using advanced land surface modeling and data assimilation techniques, in order to generate optimal fields of land surface states and fluxes. It adopts multiple advanced land surface models among which Noah is representative and proves to be reliable in climate research, hydrological studies, and environmental monitoring (Rodell et al., 2004). The GLDAS Version 2.0 were forced by the global meteorological forcing dataset from Princeton University, and generated the monthly soil moisture data at a grid size of 0.25° from 1948 to 2015. While the dataset provides soil moisture values at different depths, we selected soil moisture (kg/m^2) at 0–10 cm which was more closely related with vegetation growth (Hao et al., 2024). Annual mean soil moisture was defined as the average of monthly soil moisture within a calendar year.

Monthly VPD data from the TerraClimate product were used to calculate annual mean VPD (Abatzoglou et al., 2018). Conceptually, TerraClimate applies interpolated time-varying anomalies from CRU Ts4.0/ JRA55 (Japanese 55-year Reanalysis) to the high-spatial resolution climatology of WorldClim to create a high-spatial resolution dataset that covers a broader temporal record. The data spans the period from 1958 to 2020, with a spatial resolution of approx. 4 km (~1/24 degree). Annual mean VPD was defined as the average of monthly VPD within a calendar year.

Annual mean solar radiation was calculated from monthly surface downward solar radiation of the ERA5-Land data. ERA5-Land is a replay of the land component of the ERA5 climate reanalysis, providing a consistent view of the evolution of land variables over several decades at an enhanced resolution (9 km vs 31 km in ERA5)(Muñoz-Sabater et al., 2021). The data covers the period from 1950 to the present with a spatial resolution of approx. 9 km, and could be freely downloaded from the Climate Data Store (https://cds.climate.copernicus.eu). Annual mean solar radiation was defined as the average of monthly values within a calendar year.

Other data included the eco-geographical zones (Wu et al., 2003) and vegetation types of China. The Chinese vegetation type data were acquired from the National Cryosphere and Desert Data Center (https://www.ncdc.ac.cn/portal/). The nearest neighbor interpolation method was used to resample all datasets to the resolution of 0.0833° to be consistent with NDVI data. This method has been widely used in previous studies to resample climate data (Brandsma and Können, 2006; Piao et al., 2022). Compared to other resampling methods such as bilinear or cubic, the nearest neighbor method has higher computation efficiency when analyzing large-size data. Moreover, when downscaling the climate data, the use of this method is equivalent to assigning the fine grids with the same values of their belonged coarse gird so that the pattern of raw climate data is maintained to the largest extent.

2.2. Methods

2.2.1. PARTS method

We used the PARTS method to analyze the spatiotemporal patterns of greenness trends in China and the impacts of climate change at the map scale. The PARTS method mainly consists of two steps: first, by using an autoregressive model, PARTS derives the trend for each pixel in the time series; second, PARTS conducts map-scale hypotheses about the relation between per-pixel trends and independent variables by performing a generalized least square (GLS) regression that takes into account the spatial autocorrelation structure (Ives et al., 2021; Ives et al., 2022).

2.2.1.1. Pixel-level autoregressive trend analysis in PARTS. The trends of greenness and climate factors at the pixel level were calculated using an autoregressive (AR) model in PARTS (Ives et al., 2021), which was expressed in Eqs. (2) and (3):

$$y_i(t) = a_i + c_i t + \varepsilon_i(t) \tag{2}$$

$$\varepsilon_i(t) = \beta_i \varepsilon_i(t-1) + \delta_i(t) \tag{3}$$

where $y_i(t)$ represents dependent variable of pixel i in year t (e.g., greenness, annual mean temperature), a_i is the intercept, and c_i is the regression coefficient that reflects the rate of change. Since the time series was often temporally autocorrelated, the residuals $\varepsilon_i(t)$ were further modeled using a first-order autocorrelation model. β_i represents the autocorrelation coefficient, and $\delta_i(t)$ is Gaussian white noise with a mean of 0 and a variance of σ^2. The Restricted Maximum Likelihood (REML) estimation was used to fit the model (Ives et al., 2010). The trends of greenness (*ndvi.t*), annual mean temperature (*tmp.t*), annual precipitation (*pre.t*), annual mean vapor pressure deficit (*vpd.t*), annual mean soil moisture (*sm.t*), annual mean solar radiation (*ssr.t*) for each pixel were calculated using this model.

2.2.1.2. GLS regression analysis in PARTS. PARTS conducts a GLS regression model that accounts for spatial autocorrelation structure to test the map-scale hypotheses about the patterns of greenness trends and their relationships with climate change (Ives et al., 2021). The model could be expressed in Eq. (4) as:

$$c_i = b_0 + b_1 w_{i1} + \cdots + b_p w_{ip} + \gamma_i \tag{4}$$

where c_i represents the dependent variable, and here can be greenness trend of pixel i. w_{ip} is the independent variable p for pixel i, and b_p represents its regression coefficient. The independent variables can be variables showing environmental background, such as vegetation types, or multi-year annual mean temperature, or variables showing the long-term climate trends, such as the trends of annual mean temperature (*tmp.t*) and annual precipitation (*pre.t*). Spatial error γ_i follows a multivariate Gaussian distribution, $N(0, \sigma_\gamma^2 V)$.

GLS regression represents the spatial autocorrelation between pixel trends c_i and c_j by a spatial correlation matrix V. The matrix V is obtained by fitting the correlation of the residuals from the AR trend analysis between pairs of pixels ($cor\left[\gamma_i, \gamma_j\right]$). The commonly used distance decay function was used to model the correlation between pixel i and pixel j as shown in Eq. (5):

$$v(d_{ij}) = e^{-\left(-d_{ij}/r\right)^g} \tag{5}$$

where d_{ij} represents the distance between pixels i and j, r is the range, and g controls the shape of the function as it decreases with distance. The parameter g is often set to 2 so that the function follows a Gaussian distribution (Ives et al., 2022). Since the measurement errors of the time series for individual pixels can manifest as local variations, the nugget effect should also be considered (Ives et al., 2021). Thus, the spatial correlation matrix V can be further expressed in Eq. (6) as:

$$V = (1 - nugget)V(D) + nuggetI \tag{6}$$

D is the correlation matrix among N pixels, I is the identity matrix, and *nugget* represents the nugget. The detailed description of PARTS method could be found in Ives et al., (2021, 2022).

2.2.2. Applications of PARTS to greenness change analysis of China

PARTS method was implemented to analyze greenness trend patterns and examine their driving mechanisms under climate change at the map scale to answer the research questions proposed in Introduction (Table 1). We also conducted analyses by eco-geographical zone and vegetation type to investigate the difference in greenness trend and driving mechanism (Fig. 1). To avoid the effect of land use change, we only included in our analysis the vegetated pixels where land cover type did not change through the study period, and excluded the pixels which were classified as non-vegetated land cover type for any years (non-vegetated land), or in which land cover change occurred for any years (unstable land) (Fig.S1). The RemotePARTS package for R platform was used to implement the models, which is available at: https://doi.org/10.32614/CRAN.package.remotePARTS.

Table 1
Spatial regression models in PARTS to analyze the patterns of greenness trends and their climate effects. The dependent variable is greenness trend (*ndvi.t*). The independent variables include average greenness (*ndvi*), average annual temperature (*tmp*), average annual precipitation (*pre*), average soil moisture (*sm*), and average VPD (*vpd*) of multiple years; vegetation type (*veg_type*); eco-geographical zone (*eco_type*); the trends of annual average temperature (*tmp.t*), annual precipitation(*pre.t*), annual soil moisture (*sm.t*), annual VPD (*vpd.t*) and annual solar radiation (*ssr.t*); and their interactions. All continuous variables were standardized to have a mean of 0 and a variance of 1 so that their regression coefficients were comparable. Q1-5 represents the research questions proposed in Introduction.

Goal	Formula	Research questions
Patterns of greenness trend in China	*ndvi.t ~ 1*	What is the overall greenness trend in China? Is it significant? (Q1)
	ndvi.t ~ veg_type	What are the greenness trends of different vegetation types? Are they significantly different? (Q2)
	ndvi.t ~ eco_type	What are the greenness trends of different eco-geographical regions in China? Are they significantly different? (Q2)
Impact of environment background on greenness trend	*ndvi.t ~ ndvi + tmp + pre + sm + vpd*	Are there significant differences in the greenness change along the gradients of environmental context including *tmp*, *pre*, *sm* and *vpd*? (Q3)
Impact of climate change on greenness trends	*ndvi.t ~ ndvi + tmp + pre + sm + vpd + tmp.t + pre.t + sm.t + vpd.t + tmp.t:(tmp + pre + sm + vpd) + pre.t:(tmp + pre + sm + vpd) + sm.t:(tmp + pre + sm + vpd) + vpd.t:(tmp + pre + sm + vpd)*	How do different climate factors affect greenness trend? Do the impacts of climate change differ significantly along with environmental gradients? (Q4)
Impact of climate change on greenness trends by eco-geographical region	*ndvi.t ~ tmp.t*eco_type; ndvi.t ~ pre.t*eco_type; ndvi.t ~ vpd.t*eco_type; ndvi.t ~ sm.t*eco_type; ndvi.t ~ ssr.t*eco_type*	Do the impacts of climate change differ significantly among eco-geographical zones? How do climate factors impact greenness trend in each zone? (Q5)
Impact of climate change on greenness trends by vegetation type	*ndvi.t ~ tmp.t*veg_type; ndvi.t ~ pre.t*veg_type; ndvi.t ~ vpd.t*veg_type; ndvi.t ~ sm.t*veg_type; ndvi.t ~ ssr.t*veg_type*	Do the impacts of climate change differ significantly among different vegetation types? How do climate factors impact greenness trend in each type? (Q5)

3. Results

3.1. Patterns of greenness trends

At the pixel level, we analyzed the trends in vegetation greenness in China using AR model which accounts for temporal autocorrelation (Fig. 2). Greenness was higher in the southeast and lower in the northwest (Fig. 2a). 67 % of the pixels showed a greening trend (Fig. 2b). Specifically, 35 % of the pixels displayed a strong greening trend (*t*-test score > 2.05), while 7 % exhibited a strong browning trend (*t*-test score > 2.05). Greenness trends in the North China Plain, Loess Plateau were stronger than those in southern China, which was different from previous findings (Chen et al., 2019). The reason is that this study shows the relative trend which excludes the influence of greenness background, and makes the trends comparable among pixels (Ives et al., 2021). Also, intensive management and ecological protection project have indeed led to substantial greenness increase (Chen et al., 2019). Strong browning areas were mainly located in northern Xinjiang and some northeastern regions of China.

Spatial regression models that accounts for spatial autocorrelation were further employed to identify the overall trend of China and different vegetation types and eco-geographical regions (Table 2). The results indicate that the overall vegetation greenness in China shows a significant increasing trend, with a relative rate of 0.0012 per year ($P < 0.001$), which was consistent with previous findings (Chen et al., 2019; Piao et al., 2015). There are significant differences in the greenness trends among different vegetation types ($P < 0.001$). Except alpine meadows, subalpine shrubs and shrub deserts, other vegetation types exhibited a significant increasing trend in greenness at the significance level of 0.05 (Table 2). Among them, the temperate coniferous forests showed the largest increase. Significant differences in greenness trend were also observed among different eco-geographical zones ($P = 0.023$). Except the temperate zones and Tibetan Plateau, all other eco-geographical regions displayed a significant increasing trend in greenness ($P < 0.05$), and the warm temperate and subtropical zones showed the largest increase in greenness. The rapid greenness increase in temperate and subtropical forests benefits largely from the intensive management effect and the implementation of natural forest conservation project (NFCP) (Liao et al., 2024).

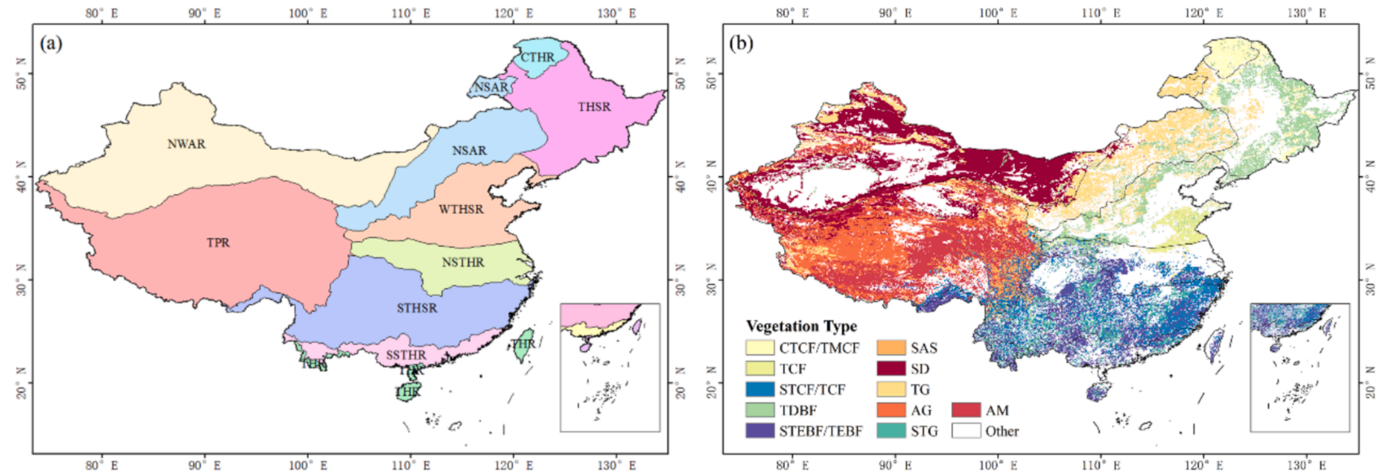

Fig. 1. Distribution of eco-geographical zones and vegetation types. (a) Eco- geographical zones including cold temperate humid region (CTHR), temperate humid/semi-humid region (THSR), warm temperate humid/semi-humid region (WTHSR), northern subtropical humid region (NSTHR), subtropical humid region (STHR), southern subtropical humid region (SSTHR), tropical humid region (THR), northern semi-arid region (NSAR), northwest arid region (NWAR), Tibetan Plateau region (TPR). (b) Vegetation types including cold temperate/temperate mountainous coniferous forests (CTCF/TMCF), temperate coniferous forests (TCF), subtropical and tropical coniferous forests (STCF/TCF), temperate deciduous broadleaf forests (TDBF), subtropical and tropical evergreen broadleaf forests (STEBF/TEBF), subalpine shrub (SAS), shrub desert (SD), temperate grassland (TG), alpine grassland (AG), subtropical grassland (STG), alpine meadow (AM).

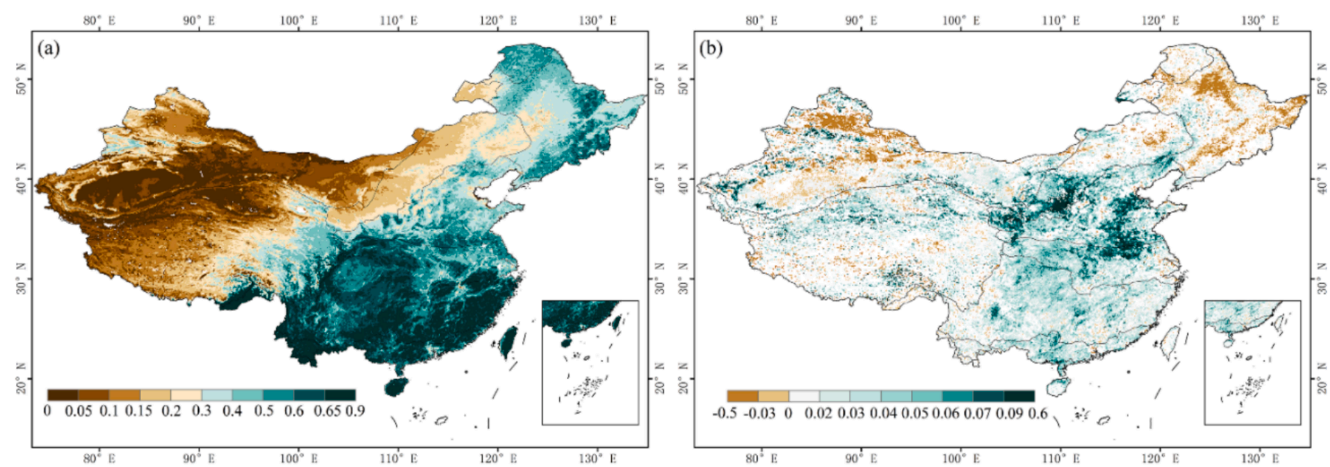

Fig. 2. Spatial patterns of multi-year greenness and greenness trends. (a) Multi-year greenness showing the average over the period 1982–2015; (b) Change trends from 1982 to 2015. An autoregressive model was applied to calculate the change trends as shown in Eq. (2). To make the trend comparable among pixels, the map showed the relative change trends, which were calculated by dividing the raw change trends by multi-year average greenness for the corresponding pixels.

3.2. Long-term climate effects on greenness trend

Based on the spatial and temporal patterns of greenness and climatic factors at the pixel scale, a spatial regression model that accounts for spatial autocorrelation was used to analyze the impact of climate change on vegetation trends (Table 1). The dependent variable was greenness trend, while the independent variables included multi-year (1982–2015) averages of temperature (*tmp*), precipitation (*pre*), soil moisture (*sm*), vapor pressure deficit (*vpd*), solar radiation (*ssr*) (Fig. 3); trends in annual mean temperature (*tmp.t*), annual precipitation (*pre.t*), annual mean soil moisture (*sm.t*), annual mean VPD (*vpd.t*), annual mean surface solar radiation (*ssr.t*) from 1982 to 2015 (Fig. 4); and their interactions. The annual VPD influenced by both temperature and air humidity, showed high values in the northwest, followed by the east, and the lowest values occurred on the Tibetan Plateau due to low temperature and arid condition (Fig. 3c). The pattern of annual soil moisture, generally consistent with the precipitation distribution, decreased from the southeast to the northwest (Fig. 3d). The solar radiation showed clear spatial variations with high values in the Northwest and on the Tibetan Plateau and low values in the Northeast and South of China (Fig. 3e). Accounting for spatial autocorrelation, *tmp.t* and *ssr.t* showed a significant increasing overall trend ($P < 0.05$) (Fig. 4). The overall trends for *pre.t*, *sm.t* and *vpd.t* were not significant ($P > 0.05$), although pixels with strong trends occurred in some regions (Fig. 4). Areas with strong increasing annual precipitation were mainly located in the west; VPD showed an increasing trend in the east; soil moisture decreased in the southeast and increased in the northwest; annual solar radiation showed a strong increasing trend in the Southeast and a strong decreasing trend in the west of the Tibetan Plateau (Fig. 4).

Environmental gradients could significantly affect greenness trend ($P < 0.001$). The greenness trend differed significantly with *ndvi* (coefficient: -0.0738; $P < 0.001$), *tmp* (coefficient: 0.0128; $P < 0.001$), *pre* (coefficient: 0.0033; $P = 0.086$), *sm* (coefficient: 0.003; $P = 0.009$), and *vpd* (coefficient: -0.0063; $P < 0.001$) (Table 3a). This suggested that in regions with lower vegetation greenness, warmer and wetter climates, and moist soils and air, the greening rate was higher. This suggests that vegetation growth is faster in favorable conditions, but could slow down when approaching or exceeding the optima (Huang et al., 2019). At the

Table 2

Trends in vegetation greenness trend by vegetation type and eco-geographical zone. The GLS model shown in Eq. (4) was used to regress greenness trend (*ndvi.t*) against vegetation types (*ndvi.t* ~ *veg_type*) and eco-geographical zones (*ndvi.t* ~ *eco_type*). * indicates that the overall trend is significant at the significance level of 0.05. CTCF/TMCF: Cold temperate/temperate mountainous coniferous forests, TCF: temperate coniferous forests, STCF/TCF: subtropical and tropical coniferous forests, TDBF: temperate deciduous broadleaf forests, STEBF/TEBF: subtropical and tropical evergreen broadleaf forests, SAS: subalpine shrub, SD: shrub desert, TG: temperate grassland, AG: alpine grassland, STG: subtropical grassland, AM: alpine meadow; CTHR: Cold temperate humid region, THSR: temperate humid/semi-humid region, WTHSR: warm temperate humid/semi-humid region, NSTHR: northern subtropical humid region, STHR: middle subtropical humid region, SSTHR: southern subtropical humid region, THR: tropical humid region, NSAR: northern semi-arid region, NWAR: northwest arid region, TPR: Tibetan Plateau region.

Vegetation type	*ndvi.t*	Eco-geographical zone	*ndvi.t*
CTCF/TMCF	0.0012*	CTHR	0.0007
TCF	0.0018*	THSR	0.0002
STCF/TCF	0.0010*	WTHSR	0.0018*
TDBF	0.0013*	NSTHR	0.0018*
STEBF/TEBF	0.0010*	STHR	0.0016*
SAS	0.0005	SSTHR	0.0021*
SD	0.0007	THR	0.0017*
TG	0.0014*	NSAR	0.0019*
AG	0.0009*	NWAR	0.0012*
SG	0.0013*	TPR	0.0006
AM	0.0007		

national scale, without accounting for interactions among variables, the trends of temperature (*tmp.t*), precipitation (*pre.t*), and VPD (*vpd.t*) did not have significant effects on the greenness trend, while the soil moisture trend (*sm.t*) was significantly and negatively correlated with the greenness trend at the significance level of 0.1 (coefficient: −0.0011, $P = 0.074$) (Table 3b). The negative correlation is supported by previous findings that vegetation greening could significantly reduce soil moisture due to enhanced evapotranspiration and leaf interception of precipitation (Li et al., 2018).

The significant effect of the interaction between factors was indicated by model comparison that the spatial regression model that included interactions significantly differed from the model without interactions (Chi-square test, $P < 0.001$). The effect of precipitation trends on greenness trends was significantly modulated by greenness levels (*ndvi*) (coefficient: −0.0192; $P = 0.021$), suggesting that in areas with lower greenness, precipitation trend had a stronger positive effect on greenness trend. In regions with high greenness, precipitation can negatively impact greenness, because excessive rainfall may prevent root respiration, reduce soil nutrition, or decrease photoperiod (Guo et al., 2020; Huete et al., 2006). The influence of VPD trend on the greenness trend significantly interacted with the level of VPD (*vpd*) condition (Table 3c). In areas with higher VPD level, the overall positive relationship between the trends of VPD and greenness was significantly enhanced. Because these regions are covered by grasslands in which a moderate increase in VPD can maintain leaf expansion, allowing leaves to absorb more CO_2 and promote photosynthesis (Yu et al., 2022). We found that soil moisture was significantly and negatively correlated with greenness trend, but its effect closely interacted with ambient environmental conditions. In regions with lower greenness, temperature and VPD, an increase in soil moisture tended to significantly decrease greenness trend. The reason is that an increase in soil moisture may be accompanied by melting permafrost and intensified soil erosion, leading to weak photosynthesis and browning trend (Li et al., 2024).

3.3. Climate impacts by vegetation type and eco-geographical zone

The impact of climate change on greenness trend for different vegetation types and eco-geographical zones was analyzed using a GLS regression model that accounts for spatial autocorrelation (Table 4 and 5). Model comparison indicated that the effects of all climate factors on greenness trends differed significantly among vegetation types (Chi-squared test; $P < 0.05$). The influence of temperature on greenness trends varied in direction and magnitude across different vegetation types (Table 4). But only in the cold temperate mountainous coniferous forest region, the temperature trend was significantly and negatively correlated with the greenness trend (coefficient: −0.006; $P = 0.063$) because of the warming-induced drought stress (D'Orangeville et al., 2018). As regarding VPD, its trend was significantly and negatively correlated with greenness trend in subtropical and tropical evergreen broadleaf forests (regression coefficient: −0.007; $P = 0.085$). The reason is that stomatal conductance is more sensitive to VPD change, and the elevated VPD could cause stomatal closure and weakened photosynthesis (Cunningham, 2005). Soil moisture trends had a significant negative correlation with trends in greenness in many ecosystems of cold regions, including cold temperate/temperate mountainous coniferous forests ($P = 0.06$), temperate coniferous forests ($P = 0.007$), subalpine shrubs ($P = 0.037$), and temperate grasslands ($P = 0.003$), which was consistent with the results for the whole China. The positive effect of solar radiation on greenness trend was stronger in temperate needleleaf forest ($P = 0.068$), and the effects on greenness trend in temperate and alpine grasslands were significantly negative ($P = 0.01$ and $P = 0.052$, respectively). The reason was that the increase in radiation could cause temperature rise in temperature-limited ecosystems (i.e., temperate needleleaf forests), and promote photosynthetic activities, while the increase could aggravate water stress in water-limited ecosystems (i.e., temperate grasslands) (Nemani et al., 2003).

Model comparison tests indicated that the effects of climate factors on greenness trends differed significantly across different eco-geographical zones (Chi-squared test; $P > 0.05$) (Table 5). Although precipitation was the main driving factor of greenness (Fensholt et al., 2012; Piao et al., 2020), only in the northern semi-arid region did precipitation changes demonstrate a significant positive effect on greenness trends (coefficient: 0.014; $P = 0.009$). In most eco-geographical zones, the VPD change showed a negative correlation with greenness trend. Notably, in arid regions of northwestern China, the trend in VPD exhibited a significantly positive correlation with greenness trends (coefficient: 0.017; $P = 0.089$). This was consistent with the above result that the positive effects of VPD was stronger in regions of higher VPD level (i.e. Northwest China). The influence of soil moisture varies in magnitude and direction across different eco-geographical zones, and the significantly negative effect of soil moisture was only observed in the north subtropical humid zone (coefficient: −0.018; $P = 0.015$) where the elevated VPD was prone to cause stomatal closure of plant, and reduced photosynthetic activities. The significantly negative effect of solar radiation change on greenness trend was found only in the northern semi-arid region ($P = 0.029$). The reason was that radiation could aggravate water stress in water-limited ecosystems (Wu et al., 2021).

Above we examined the differences in the effects of climate change among different vegetation types and eco-geographical zones separately. However, one eco-geographical zone included many vegetation types, and the effects of climate factors in different vegetation types of an eco-geographical zone might be different from those of the whole China. Given this, we made analysis for each eco-geographical zone within which the effects of climate factors in different vegetation types were examined (Fig. S2). We found that the effect directions of climate factors in different vegetation types were generally consistent between the analysis for specific eco-geographic zone and for the whole China. But the effect magnitude and significance were different because the ranges of climate variables of a specific vegetation type varied among different zones and China. Given that our goal was to understand greenness change over the entire China, we would recommend to conduct analysis by vegetation type for the whole China which could encompass the wide range of relationships.

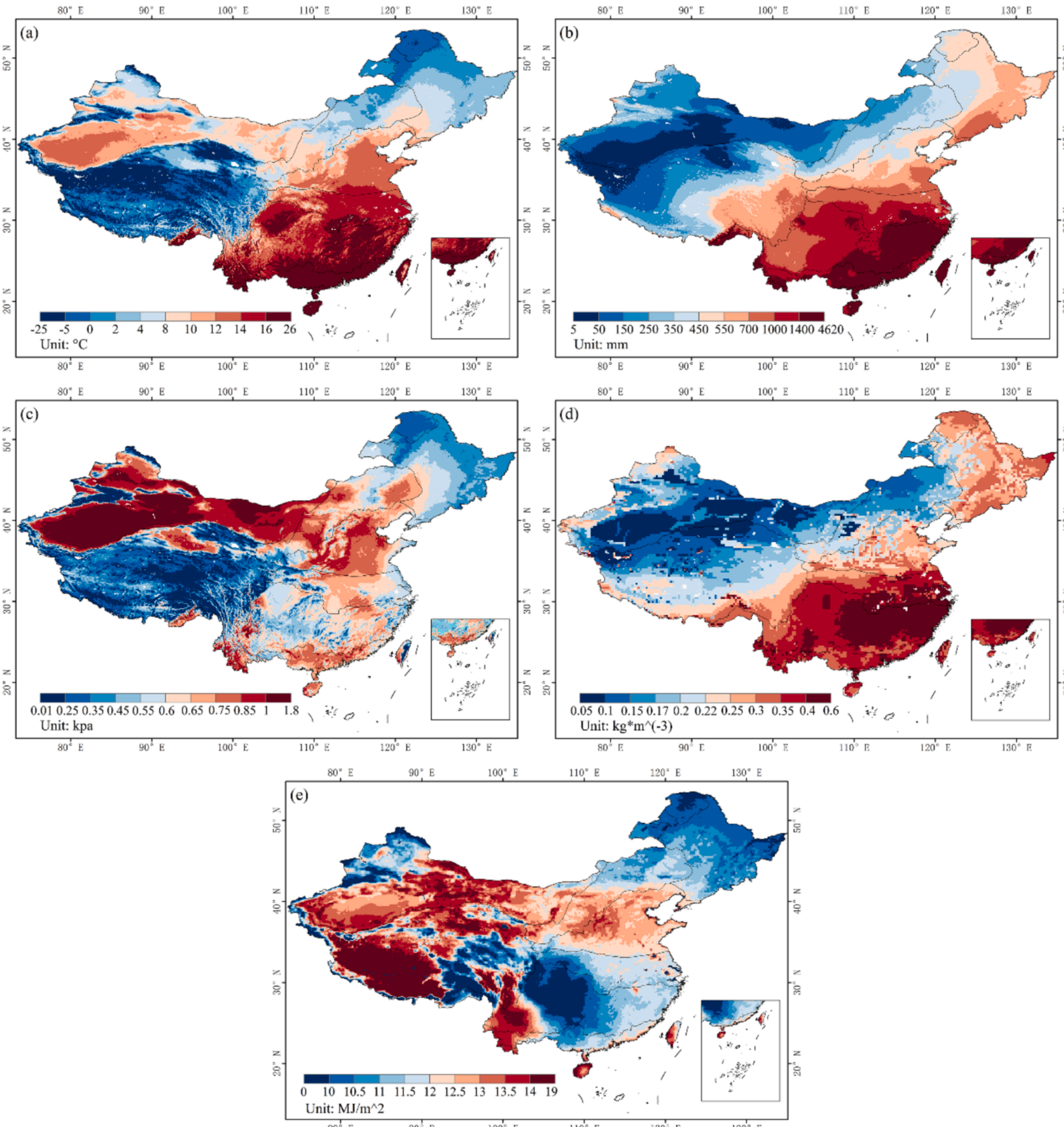

Fig. 3. Spatial patterns of multi-year values of climatic factors averaged over the period from 1982 to 2015. (a) annual mean temperature (*tmp*), (b) annual precipitation (*pre*), (c) annual mean VPD (*vpd*), (d) annual mean soil moisture (*sm*) and (e) annual mean solar radiation (*ssr*).

4. Discussion

The research analyzes the greenness trends and their climate impacts in China using the PARTS method, which can consider spatial and temporal autocorrelation and effectively integrate information from millions of pixels to test hypotheses about regional patterns. This study gains new insights into the regional patterns of greenness trends and their climate impacts which are unable to do by previous statistical methods.

This study provides an analytical framework for examining ecosystem responses to global change, which has three advantages over the current common practice. First, it effectively accounts for temporal autocorrelation in remote sensing time series to achieve lower rate of false positive trends (Cortés et al., 2021; Ives et al., 2021). Second, it aggregates information from millions of pixels and makes a rigorous statistical test for the hypothesis about regional pattern. Due to spatial autocorrelation, integrating pixel information is much more complex than analyzing a single pixel time series (Wadoux and Heuvelink, 2023), and averaging pixel information might give a false pattern (Cortés et al., 2021; Ives et al., 2021). Moreover, the models can handle huge samples of remote sensing time series, and here time series of about 120,0000 pixels were included in the model in our study. Third, it can examine the effects of long-term climate trends rather than the effects of year-to-year fluctuations, because the ecological processes governing year-to-year fluctuations and long-term trends of greenness are different (Linscheid et al., 2020; Wolkovich et al., 2012). The long-term climate trends are

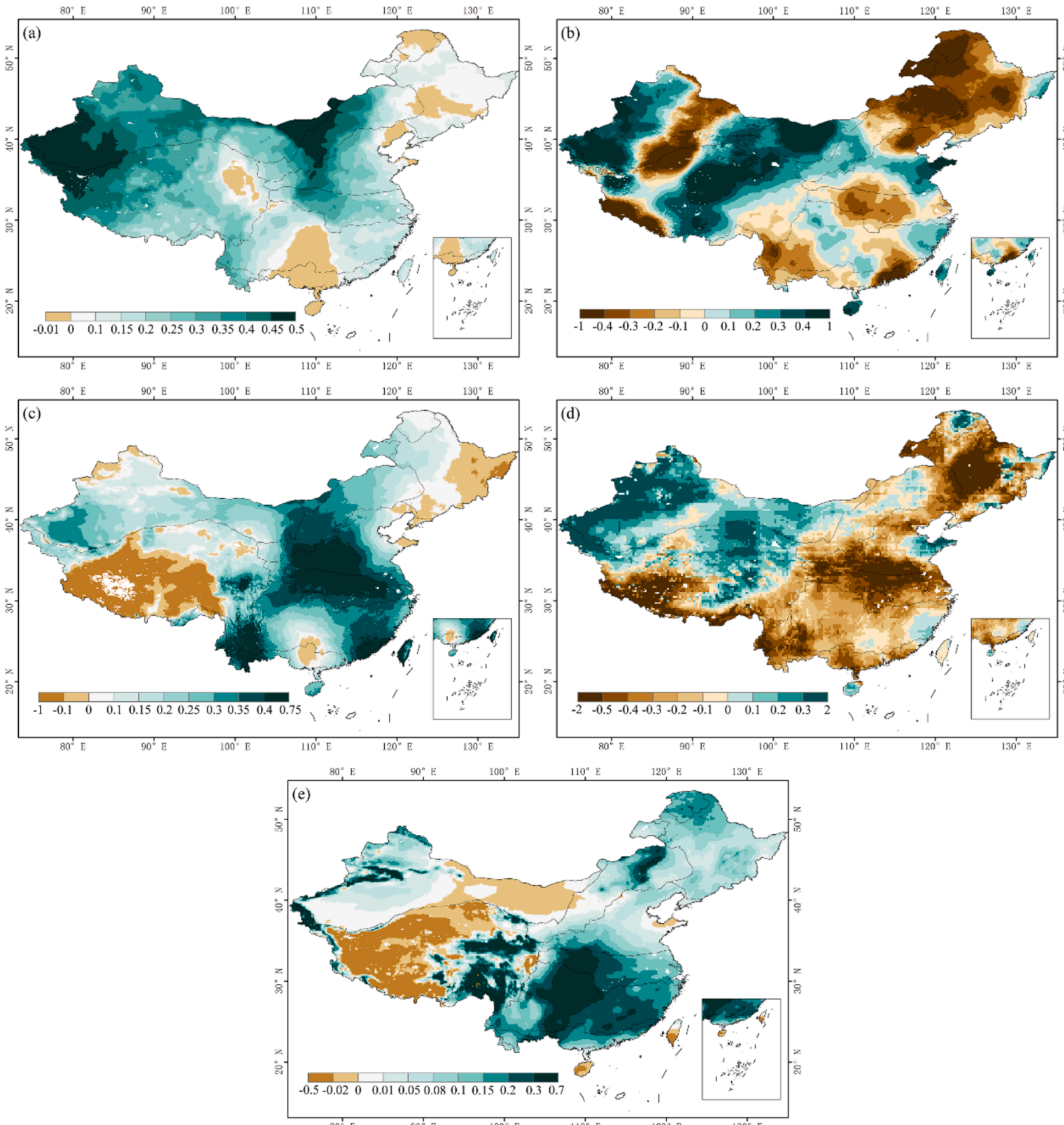

Fig. 4. Spatial patterns of the trends for climate factors from 1982 to 2015. Trends for (a) annual mean temperature (*tmp.t*), (b) annual precipitation (*pre.t*), (c) annual mean VPD (*vpd.t*), (d) annual mean soil moisture (*sm.t*) and (e) annual mean solar radiation (*ssr.t*). Trend was detected through an autoregressive model shown in Eq. (2). Except *tmp.t*, other variables are shown as relative trend, which is calculated as the raw trend value divided by the multi-year average climate factors for the corresponding pixel.

needed to be chosen as driving factors to explain greenness trend (Ives, 1995), as we did in this study.

This study provides new insights into the driving mechanisms of vegetation dynamics in China, which could also be extended to explain and predict ecosystem responses to climate change globally. First, ambient environmental conditions significantly affect the pattern of greenness change. In areas with adequate water and heat conditions (e.g., subtropical and warm temperate regions), vegetation greenness increases at a higher rate; but in regions of higher greenness (i.e., tropical forests), the greening rate slows down due to the saturation effect of NDVI or the close to temperature optima of vegetation productivity (Huang et al., 2019; Piao et al., 2020). Second, climate change significantly influences greenness trends, and their impacts interact strongly with environmental conditions. The result reveals a significant negative correlation between long-term trends of temperature and greenness, which is different from previous findings (Piao et al., 2015). There might be three reasons: (i) studies often use spatial averaging methods to uncover the relationship at the national scale, which carries much uncertainty (Wadoux and Heuvelink, 2023); (ii) this study examines the long-term relationships between the trends of climate factors and greenness, instead of the relationships between their year-to-year fluctuations; (iii) rising temperatures may aggravate water stress (Fensholt et al., 2012) or surpass optimal temperature threshold of vegetation growth (Huang et al., 2019), and further limit greenness

Table 3
Spatial regression model in PARTS to examine the climate effects on greenness trend. The dependent variable is greenness trend (*ndvi.t*), while the independent variables include multi-year averages of greenness (*ndvi*), temperature (*tmp*), precipitation(*pre*), soil moisture (*sm*), and vapor pressure deficit (*vpd*); temperature trend (*tmp.t*), precipitation trend (*pre.t*), soil moisture trend (*sm.t*); and vapor pressure deficit trend (*vpd.t*); and their interactions. The spatial regression analysis was conducted using remotePARTS package for R platform. The values of each independent variable were standardized to have a mean of 0 and a variance of 1. ***, P < 0.001; **, P < 0.01; *, P < 0.05; †, P < 0.1.

factor	*ndvi.t*	*ndvi.t*	*ndvi.t*
ndvi	−0.0738***		−0.0745***
tmp	0.0128***		0.0149***
pre	0.0033†		0.0004
sm	0.0030**		0.0023†
vpd	−0.0063***		−0.0076***
tmp.t		−0.0014	−0.0073*
tmp.t:ndvi			0.0086
tmp.t:tmp			0.0024
tmp.t:pre			−0.0024
tmp.t:sm			−0.0001
tmp.t:vpd			−0.0025
pre.t		0.0025	0.0070*
pre.t:ndvi			−0.0192*
pre.t:tmp			−0.0011
pre.t:pre			0.0035
pre.t:sm			−0.0003
pre.t:vpd			0.0013
vpd.t		−0.0013	0.0104***
vpd.t:ndvi			0.0028
vpd.t:tmp			−0.0017†
vpd.t:pre			0.0007
vpd.t:sm			0.0009
vpd.t:vpd			0.0100***
sm.t		−0.0011†	−0.0056*
sm.t:ndvi			0.0121*
sm.t:tmp			−0.0062***
sm.t:pre			0.0019
sm.t:sm			−0.0003
sm.t:vpd			0.0033*

Table 4
The impacts of climate change on greenness trend within different vegetation types. A spatial regression model in PARTS was established to analyze the difference in the climate effects on greenness trends among different vegetation types. The dependent variable is greenness trend, while the independent variables include the trends in annual mean temperature (*tmp.t*), annual precipitation (*pre.t*), annual mean VPD (*vpd.t*), annual mean soil moisture (*sm.t*), and annual mean solar radiation (*ssr.t*). CTCF/TMCF: Cold temperate/temperate mountainous coniferous forests, TCF: temperate coniferous forests, STCF/TCF: subtropical and tropical coniferous forests, TDBF: temperate deciduous broadleaf forests, STEBF/TEBF: subtropical and tropical evergreen broadleaf forests, SAS: subalpine shrub, SD: shrub desert, TG: temperate grassland, AG: alpine grassland, STG: subtropical grassland, AM: alpine meadow; * $P < 0.05$.

Vegetation	*tmp.t*	*pre.t*	*vpd.t*	*sm.t*	*ssr.t*
CTCF/TMCF	−0.006*	−0.005	−0.008	−0.003*	0.001
TCF	−0.002	−0.010	0.012	−0.016*	0.015
STCF/TCF	−0.003	−0.002	−0.004	−0.0001	0.002
TDBF	0.0001	−0.001	−0.002	0.0001	−0.004
STEBF/TEBF	−0.004	−0.004	−0.007*	−0.001	0.001
SAS	−0.001	−0.003	−0.001	−0.005*	0.001
SD	−0.004	0.003	−0.002	0.0004	−0.002
TG	−0.001	0.001	−0.001	−0.004*	−0.005*
AG	−0.001	0.002	0.001	−0.0003	−0.003
STG	−0.002	−0.002	−0.007	−0.003	−0.001
AM	−0.001	0.003	−0.001	−0.00004	0.002

increase.

Counterintuitively, the results show on average a significant negative correlation between soil moisture and greenness trend for the whole China, while VPD change exhibits a significant positive correlation with greenness trend. Generally, moderate soil moisture ensures normal transpiration and stomatal regulation in vegetation, and benefits plant growth. However, in cold areas with lower greenness, temperature and VPD, the overall negative impact of soil moisture change greenness was enhanced significantly. The reason is that an increase in soil moisture may be accompanied by melting permafrost and intensified soil erosion, leading to vegetation degradation and browning trend (Li et al., 2024; Yang et al., 2013). This result is well supported by the studies conducted in high-latitude ecosystems such as boreal forests (D'Orangeville et al., 2018). Overall, the VPD shows a positive correlation with vegetation greenness changes, but it is modulated by temperature and VPD conditions. In regions with higher temperatures and lower VPD such as tropical and subtropical evergreen broadleaf forests, VPD trend has significant and negative influence on greenness trend, because the increase in VPD is prone to close stomata, and weakens photosynthetic activity (Cunningham, 2005). This might be useful to explain the substantial damage to vegetation greenness in tropical forests caused by drought (Cunningham, 2005). We found that increasing VPD has significantly positive impacts on greenness in the arid regions of northwestern China where VPD is higher. On the one hand, vegetation are strongly tolerant to drought in this area; on the other hand, the increased water demand with increased VPD could promote the absorption of soil water by roots and water use efficiency (Yu et al., 2022; Yuan et al., 2019). With the expected increase in VPD in tropics and soil moisture at many high-latitude areas under future climate warming (Berg et al., 2017; Fang et al., 2022), ecosystems in these regions might be at high risk according to our findings, and ecosystem models should carefully account for these underlying processes to better predict future changes.

Table 5
The impacts of climate change on greenness trends within different eco-geographical zones. GLS regression model in PARTS was established to analyze the differences in the climate effects on greenness trends among different eco-geographical zones. The independent variables include the trends in annual mean temperature (*tmp.t*), annual precipitation (*pre.t*), annual mean VPD (*vpd.t*), annual mean soil moisture (*sm.t*), and annual mean solar radiation (*ssr.t*). CTHR: Cold temperate humid region, THSR: temperate humid/semi-humid region, WTHSR: warm temperate humid/semi-humid region, NSTHR: northern subtropical humid region, STHR: mid-subtropical humid region, SSTHR: southern subtropical humid region, THR: tropical humid region, NSAR: northern semi-arid region, NWAR: northwest arid region, TPR: Tibetan Plateau region. *P < 0.05.

Zones	*tmp.t*	*pre.t*	*vpd.t*	*sm.t*	*ssr.t*
CTHR	−0.012	−0.003	0.017	0.001	0.004
THSR	0.002	−0.001	0.004	0.0001	−0.017
WTHSR	−0.001	−0.002	−0.010	−0.009	−0.005
NSTHR	0.009	−0.012	−0.015	−0.018*	0.003
STHR	−0.004	−0.001	−0.011	0.003	0.003
SSTHR	−0.008	0.001	−0.012	0.002	0.001
THR	−0.005	−0.002	−0.006	−0.006	0.001
NSAR	0.005	0.014*	0.021	−0.004	−0.011*
NWAR	−0.004	0.002	0.017*	−0.001	0.004
TPR	−0.003	0.002	−0.001	0.0001	−0.001

This study has great implications for ecosystem assessment, environment management and policy making process. First, the detected greenness change patterns provide a useful indicator to track the progress towards the China's carbon neutrality goal and the sustainable development goal of "taking urgent action to combat climate change and its impacts" (SDGs GOAL 13) (Friedlingstein et al., 2023; Piao et al., 2020). The detected overall greening trend of China suggests the effectiveness of major ecological projects such as the 'grain-for-green' and the Three-North Shelter Forest projects, and the great contribution of China to the reduction in global carbon emissions (Chen et al., 2019). Second, the findings about the difference in the climate effect on greenness trend give us useful information about climate risk management. Environment managers could tailor targeted policy to promote ecological protection and restoration according to the unique driving mechanisms in different zones. For example, people in the tropics should take measures to mitigate and adapt to the severe consequence of atmospheric drought (increased VPD) on vegetation productivity (Cunningham, 2005). Third, analysis of greenness pattern is useful to better understand hydrological cycles and biodiversity pattern, and further to assess flooding risk or biodiversity loss (Ghalehteimouri et al., 2024). For example, vegetation greening could enhance evapotranspiration, re-allocate precipitation and runoff, and reduce flooding risk (Ghalehteimouri et al., 2024).

The study still has some limitations. Beyond the climatic factors in our analysis, other factors such as soil nutrient availability and extreme climates also impact vegetation greenness. Here this study did not account for soil nutrient availability. Given that the focus is to examine the trends of climate factors on greenness trend, the trends of soil nutrient are difficult to derive due to the lack of continuous dataset and the stability of soil nutrient in the study period. Anthropogenic changes in the rate and distribution of nitrogen deposition could influence greening patterns (Piao et al., 2020), but much effort is still needed to elucidate the complex processes underlying the effect of nitrogen deposition on plants. Extreme climate event could cause sudden decrease in time series of greenness. But this does not influence the results about the impacts of the trends in climate factors on greenness trends. Because the used method could identify the trend correctly even when a sudden shock in time series occurred (Ives et al., 2021). We did not consider the lag effect of climate change on vegetation growth that especially matters for intra-annual plant fluctuations (Lian et al., 2021; Shen et al., 2022; Wu et al., 2015). The climate data used in this study may be biased in some areas where is no station measurements for interpolation.

5. Conclusions

This study uses the PARTS method that accounts for temporal and spatial autocorrelation to reanalyze the patterns of greenness trend in China and the impacts of climate change. The identified patterns that undergo rigorous statistical tests are reliable, and provide new insights into vegetation dynamics in China. There is a significant overall increasing trend in vegetation greenness in China from 1982 to 2015. However, greenness trends differ significantly among vegetation types and eco-geographical regions ($P < 0.05$). The greenness trends are significantly influenced by environmental conditions, long-term climate change, and their interactions. Temperature does not make significant effect independently, but shows strong interactions with other climatic factors. As expected, precipitation has significant impacts on greenness in arid areas. The relationship between VPD change and greenness trend was significantly positive in the northwestern arid regions but negative in the tropical and subtropical areas. The negative effect of soil moisture on greenness trend was significant in the ecosystems of cold regions. Global warming has made widespread and profound impacts on ecosystems, and given that the warming trend will continue, the findings in this study is of great importance to predict the future effects of global climate change on vegetation dynamics. While the volume and complexity of remote sensing data necessitates more cautious analysis to identify underlying patterns, our study offers a new methodological framework for analysis of remote sensing time series for global change research.

CRediT authorship contribution statement

Lingwei Chen: Writing – original draft, Methodology, Investigation, Formal analysis, Data curation, Conceptualization. **Likai Zhu:** Writing – review & editing, Methodology, Investigation, Funding acquisition, Formal analysis, Data curation, Conceptualization. **Cuiyutong Yang:** Writing – review & editing, Methodology, Investigation, Formal analysis. **Zizhen Dong:** Writing – review & editing, Methodology, Investigation, Formal analysis. **Rui Huang:** Writing – review & editing, Methodology, Investigation, Formal analysis. **Jijun Meng:** Writing – review & editing, Funding acquisition, Conceptualization. **Min Liu:** Writing – review & editing, Project administration, Methodology, Investigation, Funding acquisition, Formal analysis, Conceptualization.

Declaration of competing interest

The authors declare that they have no known competing financial interests or personal relationships that could have appeared to influence the work reported in this paper.

Acknowledgements

This study was supported by the International Research Center of Big Data for Sustainable Development Goals [Grant No. CBAS2022GSP07], the National Natural Science Foundation of China [Grant No. 42001373 and 42230506], and Director's Fund of Key Laboratory of Geographic Information Science (Ministry of Education), East China Normal University (Grant No. KLGIS2023C03).

Appendix A. Supplementary data

Supplementary data to this article can be found online at https://doi.org/10.1016/j.jag.2025.104548.

Data availability

Data will be made available on request.

References

Abatzoglou, J.T., Dobrowski, S.Z., Parks, S.A., Hegewisch, K.C., 2018. TerraClimate, a high-resolution global dataset of monthly climate and climatic water balance from 1958-2015. Scientific Data 5, 170191.
Bennett, E.M., Peterson, G.D., Gordon, L.J., 2009. Understanding relationships among multiple ecosystem services. Ecology Letter 12, 1394–1404.
Berg, A., Sheffield, J., Milly, P.C.D., 2017. Divergent surface and total soil moisture projections under global warming. Geophysical Research Letters 44, 236–244.
Brandsma, T., Können, G.P., 2006. Application of nearest-neighbor resampling for homogenizing temperature records on a daily to sub-daily level. International Journal of Climatology 26, 75–89.
Chen, C., Park, T., Wang, X., Piao, S., Xu, B., Chaturvedi, R.K., Fuchs, R., Brovkin, V., Ciais, P., Fensholt, R., 2019. China and India lead in greening of the world through land-use management. Nature Sustainability 2, 122–129.
Chen, J., Jönsson, P., Tamura, M., Gu, Z., Matsushita, B., Eklundh, L., 2004. A simple method for reconstructing a high-quality NDVI time-series data set based on the Savitzky–Golay filter. Remote Sensing of Environment 91, 332–344.
Cortés, J., Mahecha, M.D., Reichstein, M., Myneni, R.B., Chen, C., Brenning, A., 2021. Where Are Global Vegetation Greening and Browning Trends Significant? Geophysical Research Letters 48, e2020GL091496.
Cunningham, S.C., 2005. Photosynthetic responses to vapour pressure deficit in temperate and tropical evergreen rainforest trees of Australia. Oecologia 142, 521–528.
D'Orangeville, L., Houle, D., Duchesne, L., Phillips, R.P., Bergeron, Y., Kneeshaw, D., 2018. Beneficial effects of climate warming on boreal tree growth may be transitory. Nature Communications 9, 3213.
de Beurs, K.M., Henebry, G.M., 2007. A statistical framework for the analysis of long image time series. International Journal of Remote Sensing 26, 1551–1573.
DeFries, R., 2008. Terrestrial Vegetation in the Coupled Human-Earth System: Contributions of Remote Sensing. Annual Review of Environment and Resources 33, 369–390.
Fang, Z., Zhang, W., Brandt, M., Abdi, A.M., Fensholt, R., 2022. Globally Increasing Atmospheric Aridity Over the 21st Century. Earth's Future 10, e2022EF003019.
Fensholt, R., Langanke, T., Rasmussen, K., Reenberg, A., Prince, S.D., Tucker, C., Scholes, R.J., Le, Q.B., Bondeau, A., Eastman, R., Epstein, H., Gaughan, A.E., Hellden, U., Mbow, C., Olsson, L., Paruelo, J., Schweitzer, C., Seaquist, J., Wessels, K., 2012. Greenness in semi-arid areas across the globe 1981–2007 — an Earth Observing Satellite based analysis of trends and drivers. Remote Sensing of Environment 121, 144–158.
Friedlingstein, P., O'Sullivan, M., Jones, M.W., Andrew, R.M., Bakker, D.C.E., Hauck, J., Landschützer, P., Le Quéré, C., Luijkx, I.T., Peters, G.P., Peters, W., Pongratz, J., Schwingshackl, C., Sitch, S., Canadell, J.G., Ciais, P., Jackson, R.B., Alin, S.R., Anthoni, P., Barbero, L., Bates, N.R., Becker, M., Bellouin, N., Decharme, B., Bopp, L., Brasika, I.B.M., Cadule, P., Chamberlain, M.A., Chandra, N., Chau, T.-T.-T., Chevallier, F., Chini, L.P., Cronin, M., Dou, X., Enyo, K., Evans, W., Falk, S., Feely, R. A., Feng, L., Ford, D.J., Gasser, T., Ghattas, J., Gkritzalis, T., Grassi, G., Gregor, L., Gruber, N., Gürses, Ö., Harris, I., Hefner, M., Heinke, J., Houghton, R.A., Hurtt, G.C., Iida, Y., Ilyina, T., Jacobson, A.R., Jain, A., Jarníková, T., Jersild, A., Jiang, F.,

Jin, Z., Joos, F., Kato, E., Keeling, R.F., Kennedy, D., Klein Goldewijk, K., Knauer, J., Korsbakken, J.I., Körtzinger, A., Lan, X., Lefèvre, N., Li, H., Liu, J., Liu, Z., Ma, L., Marland, G., Mayot, N., McGuire, P.C., McKinley, G.A., Meyer, G., Morgan, E.J., Munro, D.R., Nakaoka, S.-I., Niwa, Y., O'Brien, K.M., Olsen, A., Omar, A.M., Ono, T., Paulsen, M., Pierrot, D., Pocock, K., Poulter, B., Powis, C.M., Rehder, G., Resplandy, L., Robertson, E., Rödenbeck, C., Rosan, T.M., Schwinger, J., Séférian, R., Smallman, T.L., Smith, S.M., Sospedra-Alfonso, R., Sun, Q., Sutton, A.J., Sweeney, C., Takao, S., Tans, P.P., Tian, H., Tilbrook, B., Tsujino, H., Tubiello, F., van der Werf, G. R., van Ooijen, E., Wanninkhof, R., Watanabe, M., Wimart-Rousseau, C., Yang, D., Yang, X., Yuan, W., Yue, X., Zaehle, S., Zeng, J., Zheng, B., 2023. Global Carbon Budget 2023. Earth System Science Data 15, 5301–5369.

Gentine, P., Green, J.K., Guérin, M., Humphrey, V., Seneviratne, S.I., Zhang, Y., Zhou, S., 2019. Coupling between the terrestrial carbon and water cycles—a review. Environmental Research Letters 14, 083003.

Ghalehteimouri, K.J., Ros, F.C., Rambat, S., 2024. Flood risk assessment through rapid urbanization LULC change with destruction of urban green infrastructures based on NASA Landsat time series data: A case of study Kuala Lumpur between 1990–2021. Ecological Frontiers 44, 289–306.

Guo, P., Zhao, X., Shi, J., Huang, J., Tang, J., Zhang, R., Chen, J., Wang, Q., Zeng, J., 2020. The influence of temperature and precipitation on the vegetation dynamics of the tropical island of Hainan. Theoretical and Applied Climatology 143, 429–445.

Hao, Y., Yuan, X., Zhang, M., 2024. Enhanced relationship between seasonal soil moisture droughts and vegetation under climate change over China. Agricultural and Forest Meteorology 358, 110258.

Huang, M., Piao, S., Ciais, P., Penuelas, J., Wang, X., Keenan, T.F., Peng, S., Berry, J.A., Wang, K., Mao, J., Alkama, R., Cescatti, A., Cuntz, M., De Deurwaerder, H., Gao, M., He, Y., Liu, Y., Luo, Y., Myneni, R.B., Niu, S., Shi, X., Yuan, W., Verbeeck, H., Wang, T., Wu, J., Janssens, I.A., 2019. Air temperature optima of vegetation productivity across global biomes. Nature Ecology and Evolution 3, 772–779.

Huete, A.R., Didan, K., Shimabukuro, Y.E., Ratana, P., Saleska, S.R., Hutyra, L.R., Yang, W., Nemani, R.R., Myneni, R., 2006. Amazon rainforests green-up with sunlight in dry season. Geophysical Research Letters 33, L06405.

Ives, A.R., 1995. Predicting the response of populations to environmental change. Ecology 76, 926–941.

Ives, A.R., Abbott, K.C., Ziebarth, N.L., 2010. Analysis of ecological time series with ARMA(p,q) models. Ecology 91, 858–871.

Ives, A.R., Zhu, L., Wang, F., Zhu, J., Morrow, C.J., Radeloff, V.C., 2021. Statistical inference for trends in spatiotemporal data. Remote Sensing of Environment 266, 112678.

Ives, A.R., Zhu, L., Wang, F., Zhu, J., Morrow, C.J., Radeloff, V.C., 2022. Statistical tests for non-independent partitions of large autocorrelated datasets. MethodsX 9, 101660.

Li, M., Cao, S., Zhu, Z., Wang, Z., Myneni, R.B., Piao, S., 2023. Spatiotemporally consistent global dataset of the GIMMS Normalized Difference Vegetation Index (PKU GIMMS NDVI) from 1982 to 2022. Earth System Science Data 15, 4181–4203.

Li, W., Yan, D., Weng, B., Lai, Y., Zhu, L., Qin, T., Dong, Z., Bi, W., 2024. Nonlinear effects of surface soil moisture changes on vegetation greenness over the Tibetan plateau. Remote Sensing of Environment 302, 113971.

Li, Y., Piao, S., Li, L.Z.X., Chen, A., Wang, X., Ciais, P., Huang, L., Lian, X., Peng, S., Zeng, Z., Wang, K., Zhou, L., 2018. Divergent hydrological response to large-scale afforestation and vegetation greening in China. Science Advances 4, eaar4182.

Lian, X., Piao, S., Chen, A., Wang, K., Li, X., Buermann, W., Huntingford, C., Penuelas, J., Xu, H., Myneni, R.B., 2021. Seasonal biological carryover dominates northern vegetation growth. Nature Communications 12, 983.

Liao, Z., Yue, C., He, B., Zhao, K., Ciais, P., Alkama, R., Grassi, G., Sitch, S., Chen, R., Quan, X., Xu, M., Wang, M., 2024. Growing biomass carbon stock in China driven by expansion and conservation of woody areas. Nature Geoscience 17, 1127–1134.

Linscheid, N., Estupinan-Suarez, L.M., Brenning, A., Carvalhais, N., Cremer, F., Gans, F., Rammig, A., Reichstein, M., Sierra, C.A., Mahecha, M.D., 2020. Towards a global understanding of vegetation–climate dynamics at multiple timescales. Biogeosciences 17, 945–962.

Miralles, D.G., Vila-Guerau de Arellano, J., McVicar, T.R., Mahecha, M.D., 2025. Vegetation-climate feedbacks across scales. Annals of the New York Academy of Sciences 1544, 27–41.

Muñoz-Sabater, J., Dutra, E., Agustí-Panareda, A., Albergel, C., Arduini, G., Balsamo, G., Boussetta, S., Choulga, M., Harrigan, S., Hersbach, H., Martens, B., Miralles, D.G., Piles, M., Rodríguez-Fernández, N.J., Zsoter, E., Buontempo, C., Thépaut, J.-N., 2021. ERA5-Land: a state-of-the-art global reanalysis dataset for land applications. Earth System Science Data 13, 4349–4383.

Nemani, R.R., Keeling, C.D., Hashimoto, H., Jolly, W.M., Piper, S.C., Tucker, C.J., Myneni, R., Running, S.W., 2003. Climate-driven increases in global terrestrial net primary production from 1982 to 1999. Science 300, 1560–1563.

Pei, Y., Dong, J., Zhang, Y., Yuan, W., Doughty, R., Yang, J., Zhou, D., Zhang, L., Xiao, X., 2022. Evolution of light use efficiency models: Improvement, uncertainties, and implications. Agricultural and Forest Meteorology 317, 108905.

Peng, S., Ding, Y., Liu, W., Li, Z., 2019. 1 km monthly temperature and precipitation dataset for China from 1901 to 2017. Earth System Science Data 11, 1931–1946.

Pettorelli, N., Vik, J.O., Mysterud, A., Gaillard, J.M., Tucker, C.J., Stenseth, N.C., 2005. Using the satellite-derived NDVI to assess ecological responses to environmental change. Trends in Ecology and Evolution 20, 503–510.

Piao, S., Wang, J., Li, X., Xu, H., Zhang, Y., 2022. Spatio-temporal changes in the speed of canopy development and senescence in temperate China. Global Change Biology 28, 7366–7375.

Piao, S., Wang, X., Park, T., Chen, C., Lian, X., He, Y., Bjerke, J.W., Chen, A., Ciais, P., Tømmervik, H., Nemani, R.R., Myneni, R.B., 2020. Characteristics, drivers and feedbacks of global greening. Nature Reviews Earth & Environment 1, 14–27.

Piao, S., Yin, G., Tan, J., Cheng, L., Huang, M., Li, Y., Liu, R., Mao, J., Myneni, R.B., Peng, S., Poulter, B., Shi, X., Xiao, Z., Zeng, N., Zeng, Z., Wang, Y., 2015. Detection and attribution of vegetation greening trend in China over the last 30 years. Global Change Biology 21, 1601–1609.

Pinzon, J., Tucker, C., 2014. A Non-Stationary 1981–2012 AVHRR NDVI3g Time Series. Remote Sensing 6, 6929–6960.

Radeloff, V.C., Dubinin, M., Coops, N.C., Allen, A.M., Brooks, T.M., Clayton, M.K., Costa, G.C., Graham, C.H., Helmers, D.P., Ives, A.R., Kolesov, D., Pidgeon, A.M., Rapacciuolo, G., Razenkova, E., Suttidate, N., Young, B.E., Zhu, L., Hobi, M.L., 2019. The Dynamic Habitat Indices (DHIs) from MODIS and global biodiversity. Remote Sensing of Environment 222, 204–214.

Rodell, M., Houser, P.R., Jambor, U., Gottschalck, J., Mitchell, K., Meng, C.J., Arsenault, K., Cosgrove, B., Radakovich, J., Bosilovich, M., Entin, J.K., Walker, J.P., Lohmann, D., Toll, D., 2004. The Global Land Data Assimilation System. Bulletin of the American Meteorological Society 85, 381–394.

Shen, M., Wang, S., Jiang, N., Sun, J., Cao, R., Ling, X., Fang, B., Zhang, L., Zhang, L., Xu, X., Lv, W., Li, B., 2022. Plant phenology changes and drivers on the Qinghai–Tibetan Plateau. Nature Reviews Earth & Environment 3, 633–651.

Shi, Y., Jin, N., Ma, X., Wu, B., He, Q., Yue, C., Yu, Q., 2020. Attribution of climate and human activities to vegetation change in China using machine learning techniques. Agricultural and Forest Meteorology 294, 108146.

Wadoux, A.M.J.C., Heuvelink, G.B.M., 2023. Uncertainty of spatial averages and totals of natural resource maps. Methods in Ecology and Evolution 14, 1320–1332.

Walker, T.W.N., Janssens, I.A., Weedon, J.T., Sigurdsson, B.D., Richter, A., Penuelas, J., Leblans, N.I.W., Bahn, M., Bartrons, M., De Jonge, C., Fuchslueger, L., Gargallo-Garriga, A., Gunnarsdottir, G.E., Maranon-Jimenez, S., Oddsdottir, E.S., Ostonen, I., Poeplau, C., Prommer, J., Radujkovic, D., Sardans, J., Sigurethsson, P., Soong, J.L., Vicca, S., Wallander, H., Ilieva-Makulec, K., Verbruggen, E., 2020. A systemic overreaction to years versus decades of warming in a subarctic grassland ecosystem. Nature Ecology and Evolution 4, 101–108.

Wolkovich, E.M., Cook, B.I., Allen, J.M., Crimmins, T.M., Betancourt, J.L., Travers, S.E., Pau, S., Regetz, J., Davies, T.J., Kraft, N.J., Ault, T.R., Bolmgren, K., Mazer, S.J., McCabe, G.J., McGill, B.J., Parmesan, C., Salamin, N., Schwartz, M.D., Cleland, E.E., 2012. Warming experiments underpredict plant phenological responses to climate change. Nature 485, 494–497.

Wu, D., Zhao, X., Liang, S., Zhou, T., Huang, K., Tang, B., Zhao, W., 2015. Time-lag effects of global vegetation responses to climate change. Global Change Biology 21, 3520–3531.

Wu, G.L., Cheng, Z., Alatalo, J.M., Zhao, J., Liu, Y., 2021. Climate Warming Consistently Reduces Grassland Ecosystem Productivity. Earth's Future 9, e2020EF001837.

Wu, S., Yang, Q., Zheng, D., 2003. Delineation of eco-geogrpahic regional system of China. Journal of Geographical Sciences 13, 309–315.

Xu, L., Myneni, R.B., Chapin Iii, F.S., Callaghan, T.V., Pinzon, J.E., Tucker, C.J., Zhu, Z., Bi, J., Ciais, P., Tømmervik, H., Euskirchen, E.S., Forbes, B.C., Piao, S.L., Anderson, B.T., Ganguly, S., Nemani, R.R., Goetz, S.J., Beck, P.S.A., Bunn, A.G., Cao, C., Stroeve, J.C., 2013. Temperature and vegetation seasonality diminishment over northern lands. Nature Climate Change 3, 581–586.

Yang, Z.-P., Gao, J.-X., Zhao, L., Xu, X.-L., Ouyang, H., 2013. Linking thaw depth with soil moisture and plant community composition: effects of permafrost degradation on alpine ecosystems on the Qinghai-Tibet Plateau. Plant and Soil 367, 687–700.

Yu, T., Jiapaer, G., Bao, A., Zheng, G., Zhang, J., Li, X., Yuan, Y., Huang, X., Umuhoza, J., 2022. Disentangling the relative effects of soil moisture and vapor pressure deficit on photosynthesis in dryland Central Asia. Ecological Indicators 137, 108698.

Yuan, W., Zheng, Y., Piao, S.L., Ciais, P., Lombardozzi, D., Wang, Y., Ryu, Y., Chen, G., Dong, W., Hu, Z., Jain, A., Jiang, C., Kato, E., Li, S., Lienert, S., 2019. Increased atmospheric vapor pressure deficit reduces global vegetation growth. Science Advances 5, eaax1396.

Zeng, Y., Hao, D., Huete, A., Dechant, B., Berry, J., Chen, J.M., Joiner, J., Frankenberg, C., Bond-Lamberty, B., Ryu, Y., Xiao, J., Asrar, G.R., Chen, M., 2022. Optical vegetation indices for monitoring terrestrial ecosystems globally. Nature Reviews Earth & Environment 3, 477–493.

Zhang, Y., Piao, S., Sun, Y., Rogers, B.M., Li, X., Lian, X., Liu, Z., Chen, A., Peñuelas, J., 2022. Future reversal of warming-enhanced vegetation productivity in the Northern Hemisphere. Nature Climate Change 12, 581–586.

Zhao, L., Dai, A., Dong, B., 2018. Changes in global vegetation activity and its driving factors during 1982–2013. Agricultural and Forest Meteorology 249, 198–209.

Zhou, L., Tucker, C.J., Kaufmann, R.K., Slayback, D., Shabanov, N.V., Myneni, R.B., 2001. Variations in northern vegetation activity inferred from satellite data of vegetation index during 1981 to 1999. Journal of Geophysical Research: Atmospheres 106, 20069–20083.

Zhu, L., Meng, J., Zhu, L., 2020. Applying Geodetector to disentangle the contributions of natural and anthropogenic factors to NDVI variations in the middle reaches of the Heihe River Basin. Ecological Indicators 117, 106545.

Zhu, Z., Piao, S., Myneni, R.B., Huang, M., Zeng, Z., Canadell, J.G., Ciais, P., Sitch, S., Friedlingstein, P., Arneth, A., 2016. Greening of the Earth and its drivers. Nature Climate Change 6, 791–795.